Bioresource Technology 316 (2020) 123919

Contents lists available at ScienceDirect

Bioresource Technology

journal homepage: www.elsevier.com/locate/biortech

Impact of cathodic electron acceptor on microbial fuel cell internal resistance

Kathryn Lawson, Ruggero Rossi, John M. Regan, Bruce E. Logan*

Department of Civil and Environmental Engineering, The Pennsylvania State University, 231Q Sackett Building, University Park, PA 16802, USA

ARTICLE INFO

Keywords:
Air cathode
Bioelectricity
Electrode potentials
Ferricyanide

ABSTRACT

Ferricyanide is often used in microbial fuel cells (MFCs) to avoid oxygen intrusion that occurs with air cathodes. However, MFC internal resistances using ferricyanide can be larger than those with air cathodes even though ferricyanide results in higher power densities. Using a graphite fiber brush cathode and a ferricyanide catholyte (FC-B) the internal resistance was 62 ± 4 mΩ m^2, with 84 ± 8 mΩ m^2 obtained using ferricyanide and a flat carbon paper cathode (FC-F) and only 51 ± 1 mΩ m^2 using a 70% porosity air cathode (A-70). The FC-B MFCs produced the highest maximum power density of all configurations examined: 2.46 ± 0.26 W/m^2, compared to 1.33 ± 0.14 W/m^2 for the A-70 MFCs. The electrode potential slope (EPS) analysis method showed that electrode resistances were similar for ferricyanide and air–cathode MFCs, and that higher power was due to the larger experimental working potential (500 ± 12 mV) of ferricyanide compared to the air cathode (233 ± 5 mV).

1. Introduction

Microbial fuel cells (MFCs) can be used to produce electrical power, with current generated from oxidation of organic matter by exoelectrogenic microorganisms on the anode, paired with reduction of a chemical at the cathode (Logan et al., 2006; Logan and Rabaey, 2012; Lovley, 2012). Oxygen is a preferred electron acceptor for the cathode reaction as its use is sustainable and renewable. Oxygen is supplied to the cathode either by using air directly (air cathode) in a single-chamber MFC, or by dissolving oxygen in water (aqueous cathode) using a two-chamber MFC. Single-chamber MFCs now commonly use activated carbon catalysts to enhance oxygen reduction kinetics, stainless steel current collectors to conduct electrons across the electrode, and diffusion layers to prevent water leakage through the cathode (Pant et al., 2010). Due to direct contact of the cathode with air, oxygen can leak in through the cathode and inhibit power generation particularly for flat anodes placed too close to the cathode (Hays et al., 2011). In addition, some exoelectrogenic microorganisms are strict anaerobes (Yilmazel et al., 2016), thus prohibiting biofilm growth on the anode if they are grown without oxygen-scavenging populations and there is oxygen contamination from the cathode. Two-chamber MFCs, that use a membrane to keep the chambers separated, have an advantage for maintaining anoxic anolyte conditions as the membrane greatly reduces oxygen crossover (Liu and Logan, 2004). However, two-chamber MFCs often have lower power densities than single-chamber systems (Logan et al., 2015; Santoro et al., 2017).

Ferricyanide ($Fe(CN)_6^{3-}$) is sometimes used as an electron acceptor in two-chambered MFCs to avoid oxygen intrusion into the anolyte, and thus to maintain anaerobic conditions, as well as to produce higher power than systems using dissolved oxygen catholytes (Logan et al., 2019). When ferricyanide is used, no cathode catalyst is needed due to favorable reaction kinetics, and therefore the construction of the cathode is easier than for MFCs using oxygen, where a catalyst is usually needed. With ferricyanide the cathode can be a plain carbon electrode, such as a piece of carbon paper or carbon felt, suspended in the ferricyanide solution. Ferricyanide catholytes are often used with pure cultures (He et al., 2014; Liu et al., 2007; Logan et al., 2019; Zhang et al., 2008; Zou et al., 2015; Zuo et al., 2008), and reported power densities can be higher than those typically obtained using dissolved oxygen as the electron acceptor, but there are no direct comparisons made in the same system with only a different catholyte. For example, two-chamber MFCs using *Geobacter sulfurreducens* PCA produced 0.015 W/m^2 with a dissolved oxygen catholyte compared to 0.53 W/m^2 (Wei et al., 2010) using ferricyanide in a different system, and power densities as high as 3.9 W/m^2 have been reported using *G. sulfurreducens* KN400 and a ferricyanide catholyte (Yi et al., 2009). Power densities as high as 3.0 W/m^2 (Ringeisen et al., 2007) to 4.4 W/m^2 (Yang et al., 2017a) have also been reported for *Shewanella oneidensis* MR-1

* Corresponding author.
E-mail address: blogan@psu.edu (B.E. Logan).

https://doi.org/10.1016/j.biortech.2020.123919
Received 23 June 2020; Received in revised form 22 July 2020; Accepted 24 July 2020
Available online 30 July 2020
0960-8524/

using ferricyanide catholytes, compared to 0.0045 W/m^2 with oxygen in a different MFC configuration (Bretschger et al., 2007). The use of ferricyanide, however, does not necessarily ensure that power densities will be higher than with oxygen, as reactor configurations will impact the internal resistance, which would affect power production (Logan et al., 2019). Thus, the specific impact of different cathodes or MFC configurations requires direct evaluation of specific electrode resistances under similar reactor conditions (Rossi et al., 2019; Rossi et al., 2020; Rossi and Logan, 2020).

When the same MFC configuration is used by different laboratories, power production should be similar. For example, maximum power densities reported for air–cathode MFCs with a common configuration of cube-shaped reactors and brush anodes produced 1.36 ± 0.20 W/m^2 in 50 mM PBS (Yang et al., 2017b). Higher power densities can be achieved with these MFCs by using better cathode catalysts (Santoro et al., 2019; Yang and Logan, 2016). When different MFCs or cathodes are used power production will be limited by: overall internal resistance, which is the sum of the resistances of the anode, cathode, and solution; and cell voltage, which is a function of the half-cell potentials of the anode and cathode. The half-cell reactions for oxygen depend on a number of factors, including the pH, partial pressure of oxygen, the specific reduction product, and the number of electrons transferred (Table 1). For typical conditions in an MFC the maximum cathode potential could vary from 138 mV to 805 mV, where a pH greater than 7 is sometimes assumed as the localized solution near the cathode can become alkaline (Popat et al., 2012; Wang et al., 2013). For ferricyanide a standard potential of 361 mV has been assumed for MFCs (Logan et al., 2006), but measured potentials in a phosphate buffer similar to that used in MFCs indicated a more accurate value would be 418 mV (O'Reilly, 1973). In an MFC, only ferricyanide (not ferrocyanide, the reduced form) is added to the catholyte so the potential of the ferricyanide-ferrocyanide couple in an MFC, estimated based on properties of other mediators at highly disproportionate concentrations (Sander et al., 2015), suggests that a reasonable approximation would be 98% ferricyanide, with a potential of 518 mV based on the Nernst equation (Table 1). While the ratio of ferricyanide to ferrocyanide will change over the course of a batch cycle, polarization data are obtained at the start of a fresh batch cycle when this ratio will be relatively constant. Analysis of air–cathode MFCs has shown that the operational half-cell reaction of activated carbon cathodes is ~470 mV (Rossi et al., 2020), indicating that both 2- and 4-electron transfer pathways can occur using this catalyst (Watson et al., 2013a; Watson et al., 2013b).

The impact of the cathode reaction, i.e. using oxygen or ferricyanide, has not been previously examined in two-chamber MFCs relative to possible impacts on anode performance that could arise due to differences in current densities between reactors or the potential presence of dissolved oxygen. An impact of MFC configuration, where a reverse electrodialysis stack was placed between the electrodes, showed that the presence of the stack substantially reduced overall internal resistance leading to a marked improvement in anode performance (Cusick et al., 2013; Cusick et al., 2012). In addition to a possible impact of the cathode on the anode performance, the solution resistances in ferricyanide MFCs have not been compared to those with air cathodes. Ferricyanide MFCs have both an anolyte and catholyte solution resistance, as well as a membrane resistance, while air–cathode MFCs have only the anolyte solution resistance. Therefore, it is not known to what extent the use of ferricyanide impacts anode performance or overall internal resistance. Such information on the impact of ferricyanide on MFC performance is important for laboratory studies where ferricyanide is used, although it is not likely that ferricyanide catholytes would be used for practical applications in wastewater treatment.

In order to examine the impact of using ferricyanide on the performance of MFCs versus oxygen reduction at the cathode, we examined power production in commonly used cube-type MFCs operated in a two-chamber configuration using ferricyanide, and compared their performance to single-chamber air–cathode MFCs. MFCs with ferricyanide had either a flat carbon paper or a graphite fiber brush cathode, with performance of the flat cathode also examined using a stirred catholyte to reduce mass transfer resistances. The air cathodes used activated carbon catalysts with two different diffusion layer porosities (30% and 70%). The resistances of the individual components and the working half-cell potentials were examined using the electrode potential slope (EPS) method (Rossi et al., 2019; Rossi et al., 2020; Rossi and Logan, 2020).

2. Materials and methods

2.1. Reactor configurations and operation

MFCs were cube-shaped, polycarbonate reactors with cylindrical inside chambers (3 cm diameter, 4 cm long, liquid volume of 26 mL) commonly used in MFC studies (Yang et al., 2017b). Reactor chambers were bolted together with end plates holding the electrodes. The MFCs had the same anode chamber and electrode but different cathode configurations. Anodes were graphite carbon brushes (2.5 cm diameter, with a brush length of 2.5 cm), wrapped and held with titanium wire (Mill-Rose, Mentor, OH). Brushes were pretreated at 450 °C for 30 min to remove any impurities and increase surface area prior to use (Feng et al., 2010).

Two types of cathodes were used in different configurations, with tests run in duplicate (Fig. 1). For experiments using a ferricyanide catholyte, the cathode was either a plain brush (FC-B) or a flat circle of carbon paper (FC-F) in a second chamber identical to the anode chamber. In some tests the catholyte with the flat cathode was mixed using a stir bar and a magnetic stir plate (FC-F-S). The chambers were separated by a cation exchange membrane (CEM; Selemion, Bellex International Corporation, Wilmington, DE). For experiments using an air cathode, a single chamber was used. Air cathodes (VITO, Mol, Belgium) were made using a stainless steel mesh current collector, activated carbon, and a polytetrafluoroethylene (PTFE) diffusion layer with either 30% (A-30) or 70% (A-70) porosity. Prior to polarization tests, a Ag/AgCl reference electrode (model RE-5B, BASi; + 0.209 V vs a standard hydrogen electrode, SHE) was inserted into each chamber (Fig. 1). Measured distances between anodes, cathodes, and reference electrodes, used to calculate solution resistances, are summarized in the Supporting Information (Table A1). The anolyte contained 1 g/L sodium acetate as the electron donor in 50 mM phosphate buffer solution (PBS; 4.58 g/L Na_2HPO_4, 2.45 g/L NaH_2PO_4, 0.31 g/L NH_4Cl, and 0.13 g/L KCl) with 12.5 mL/L of concentrated trace minerals and 5 mL/L of concentrated vitamins (conductivity of 7.5 mS/cm) (Yang et al.,

Table 1
Potentials for cathodic reactions under standard conditions (E_0) compared to those adjusted for typical conditions in a microbial fuel cell (E_{MFC}). (Adapted from half-cell reactions given for MFCs (Logan et al., 2006; Rossi et al., 2020), with the ferricyanide standard reaction potential in a phosphate buffer (O'Reilly, 1973).)

Reaction	E_0 (mV)	Conditions	E_{MFC} (mV)
$O_2 + 4H^+ + 4\ e^- \rightarrow 2\ H_2O$	1229	pO_2 = 0.2, pH = 7	805
$O_2 + 4H^+ + 4\ e^- \rightarrow 2\ H_2O$	1229	pO_2 = 0.2, pH = 10	627
$O_2 + 2H^+ + 2\ e^- \rightarrow H_2O_2$	695	pO_2 = 0.2, H_2O_2 = 5 mM, pH = 7	238
$O_2 + 2H_2O + 2\ e^- \rightarrow H_2O_2 + 2\ OH^-$	–146	pO_2 = 0.2, H_2O_2 = 5 mM, pH = 10	138
$Fe(CN)_6^{3-} + e^- \rightarrow Fe(CN)_6^{4-}$	418	$Fe(CN)_6^{3-}$ = 49 mM, $Fe(CN)_6^{4-}$ = 1 mM	518

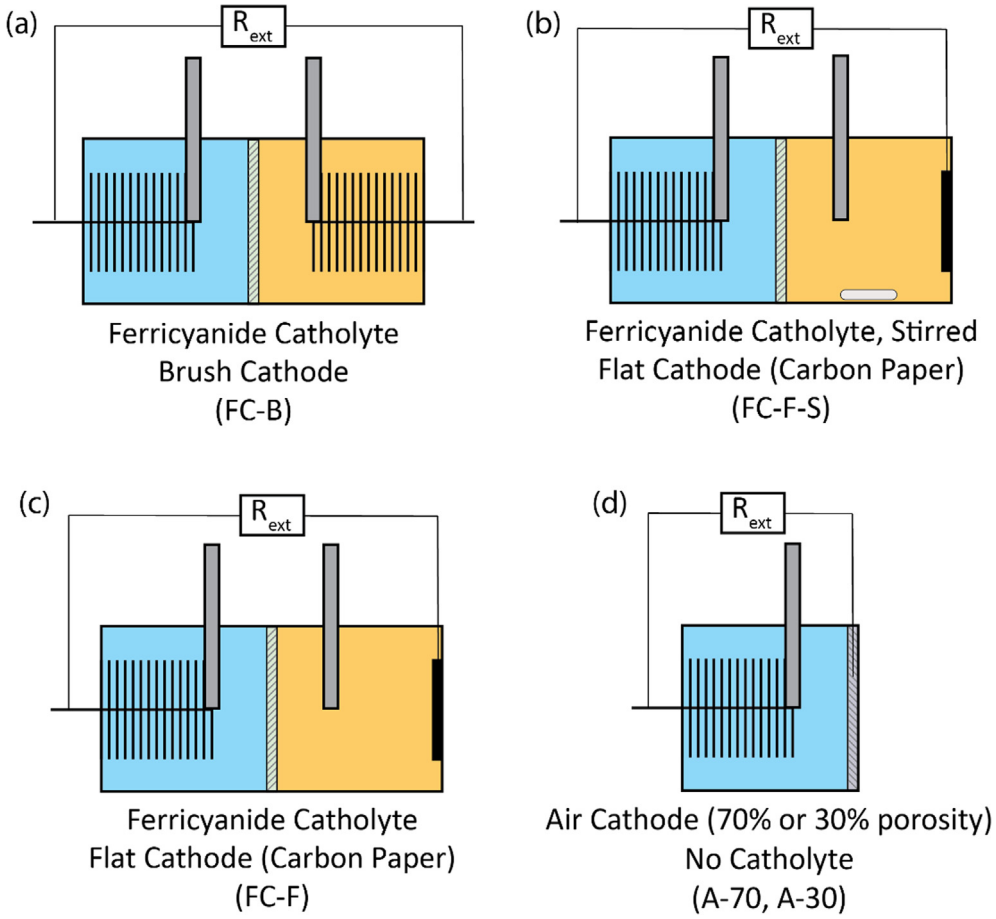

Fig. 1. MFC reactor side views, with ferricyanide catholyte (FC) or air cathodes (A). Long grey rectangles indicate reference electrode positions.

2017b). The catholyte contained 50 mM potassium ferricyanide in 50 mM PBS (conductivity 23.5 mS/cm). Reactors were inoculated using the effluent of MFCs fed the same medium mixed with an equal amount of acetate medium for several cycles and then switched to only the acetate medium. MFCs were considered to be fully acclimated based on measuring multiple reproducible cycles of current generation. The anolyte and catholyte were replaced when the measured cell voltage dropped below 10% of the cycle maximum, with voltages recorded using a multimeter and a data acquisition system (Keithley Instruments Model 2700, Cleveland, OH, USA).

2.2. Polarization tests

Duplicate reactors were normally operated with an external resistance of 1000 Ω in a constant temperature room set at 30 °C. Prior to polarization tests MFCs were acclimated for two days to lower set resistances (20–500 Ω) to minimize the potential for power overshoot (Hong et al., 2011; Watson and Logan, 2011) as it is known that acclimation to different external resistances can impact subsequent power production (Katuri et al., 2011; Koók et al., 2020; Pasternak et al., 2018; Rismani-Yazdi et al., 2011). The electrolytes were then replaced, and the reactors left in open circuit for two hours prior to conducting polarization tests by changing the external resistance (1000 Ω, 500 Ω, 200 Ω, 100 Ω, 75 Ω, 50 Ω, and 20 Ω) every 20 min. Tests were repeated until power overshoot was minimal or not observed.

2.3. Data analysis

Current density (A/m^2) was calculated as $i = U/RA$, and power density (mW/m^2) as $P = U^2/RA$, where U is the measured potential difference, R the external resistance, and A the projected (cross-sectional) area of the cathode (7 cm^2). Electrode potentials measured versus reference electrodes were adjusted to exclude solution resistance between the working and reference electrodes (Logan et al., 2018). All potentials are reported versus SHE.

The electrode resistances and experimental working potentials of the whole cell and individual electrodes were calculated using the EPS method (Rossi et al., 2019; Rossi et al., 2020; Rossi and Logan, 2020). For this method the slope of the whole cell polarization data, in the region of maximum power, is fit with a linear equation $U = |R|\, i + E$, where U is the voltage, i the current density (A/m^2), R (absolute value) is the internal resistance calculated from the slope of the line (R_{int}, mΩ m^2), and E is the working whole cell potential ($E_{wc,e0}$, V) calculated from the y-intercept (Fig. 2a). The value of $E_{wc,e0}$ is less than the measured open circuit potential ($E_{wc,m0}$) due to activity losses in potential at low current densities. The same approach is used to calculate the resistance of the anode (R_{An}) or cathode (R_{Cat}), with the y-intercepts used to calculate the experimental open circuit potentials of the anode ($E_{An,e0}$) or cathode ($E_{Cat,e0}$) (Fig. 2a).

The solution resistance (R_Ω) was obtained from the solution conductivity (σ, mS/cm) as $R_\Omega = 10^3 l/\sigma A$, where A is the cross-sectional area between the electrodes (cm^2), 10^3 is to convert mS into S (where 1 S = Ω^{-1}), and l is the distance between the electrodes (cm) (Rossi et al., 2019). The membrane resistance was calculated as the difference between the sum of the individual resistances and the measured internal resistance of the reactor (R_{int}) based on the whole cell polarization data, or (Cario et al., 2019) as:

$$R_{mem} = R_{int} - (R_{an} + R_{cat} + R_{sol}) \quad (1)$$

The membrane resistance is usually small and therefore it may have

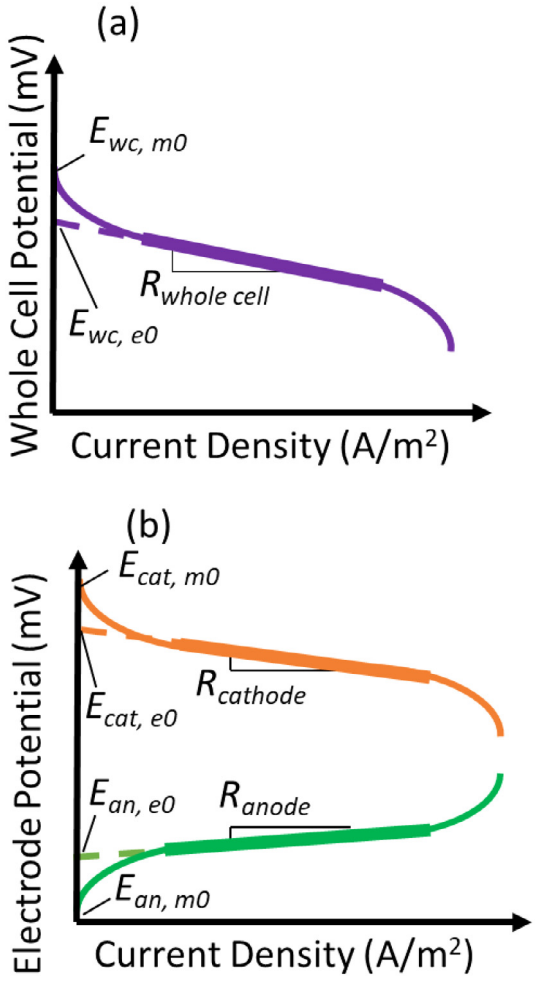

Fig. 2. Components of polarization curves for (a) whole cell and (b) individual electrodes, with examples of linearized portions shown in a bold line, and the calculated slopes and intercepts shown based on the linearized portions of the curves.

slightly positive or negative values based on errors for the slopes used to calculate the other resistances, or slight differences in electrode distances which impact the accuracy of the solution resistance (Logan et al., 2018).

3. Results and discussion

3.1. Reactor comparisons using polarization and power density curves

Analysis of performance based on power density curves showed that all ferricyanide MFCs produced higher power densities than the air–cathode MFCs (Fig. 3a). The power densities for the ferricyanide catholytes were a function of the configuration used, with the highest maximum power density of 2.46 ± 0.26 W/m^2 obtained using brush cathodes (FC-B), followed by MFCs with flat cathodes and stirred catholyte (FC-F-S, 1.98 ± 0.28 W/m^2), then MFCs with flat cathodes and static catholyte (FC-F, 1.76 ± 0.12 W/m^2). For the air–cathode MFCs, the maximum power density using the 70% porosity air cathodes was 1.33 ± 0.14 W/m^2 (A-70), which was slightly greater than that of the 30% porosity cathodes (A-30, 0.97 ± 0.07 W/m^2). The ferricyanide MFCs all had similar and higher open circuit potentials (812 ± 1 mV, FC-F-S; 798 ± 12 mV, FC-F; 778 ± 31 mV, FC-B) than the air–cathode MFCs (685 ± 22 mV, A-30; 620 ± 24 mV, A-70 (Fig. 3b).

The differences in the power densities between the ferricyanide and air–cathode MFCs were due to the working potentials of the different cathodes (Fig. 3c). The anode potentials were similar for all the reactors, with comparable open circuit potentials and a nearly linear slope of the polarization data for all current densities < 8 A/m^2 (Supporting information). Cathode potentials were generally linear over the range of measured values for the ferricyanide MFCs except for the static catholyte condition, which showed a drop off at current densities > 5 A/m^2 (Fig. 3c). The stirred flat cathodes did not exhibit this decrease, suggesting the static cathode decrease in potential was due to mass transfer limitations. The cathodes in the air–cathode MFCs showed relatively rapid decreases at low current densities indicating large activation losses.

3.2. Analysis of electrode potentials using the EPS analysis

The experimental open circuit potentials for the whole cells ($E_{WC,e0}$) were similar for all the ferricyanide MFCs (755 to 773 mV), and significantly higher than those of the air–cathode MFCs (517 ± 6 mV, A-70; and 502 ± 25 mV, A-30) (Fig. 4a). These different potentials indicated a fundamental difference between using ferricyanide or oxygen, with small differences among the three different configurations for the ferricyanide or the two air–cathode materials. The differences in the experimental open circuit potentials (the *y*-intercepts in electrode potential linearized data) for the two electron acceptors were larger than differences in measured open circuit potentials of 150 mV, with 800 ± 20 mV for the ferricyanide reactors, compared to 650 ± 50 mV for the air–cathode MFCs. This greater difference in working potentials was due to the large decrease in the air–cathode potentials at low current densities due to activation losses, compared to the ferricyanide cathodes which had relatively low activation potential losses.

Analysis of the electrode potentials showed that the working potentials of the three ferricyanide cathodes, which averaged $E_{Cat,e0}$ = 500 ± 12 mV (511 ± 5 mV, FC-B; 488 ± 2 mV, FC-F-S; and 502 ± 22 mV, FC-S), were ~270 mV larger than for the average air cathode $E_{Cat,e0}$ = 233 ± 5 (237 ± 1 mV, A-70; 230 ± 23 mV, A-30). The working potential for the cathodes in ferricyanide of $E_{Cat,e0}$ = 500 ± 12 mV (n = 3) was in reasonable agreement with that estimate based on the assumption of 98% ferricyanide (518 mV) (Table 1). For the air–cathode MFCs, the $E_{Cat,e0}$ = 233 ± 5 mV (vs SHE) was slightly higher than the potentials of two-electron transfer reactions for oxygen reduction (138 and 238 mV, Table 1).

3.3. Analysis of electrode and component resistances using the EPS method

The internal resistances of the five different reactor configurations varied widely, with the ferricyanide MFCs all having higher internal resistances than air–cathode MFCs (Fig. 5). The lowest internal resistance among the ferricyanide MFCs was obtained for the brush cathode configuration, with 62 ± 4 mΩ m^2, followed by the stirred flat cathode MFCs (73 ± 3 mΩ m^2, FC-F-S) and the still flat cathode MFCs (84 ± 8 mΩ m^2). The 70% porosity air–cathode MFCs (A-70) had the lowest internal resistance of 51 ± 1 mΩ m^2. The MFCs with the less porous diffusion layer (A-30) had an internal resistance of 62 ± 6 mΩ m^2, which was the same as that of the best performing ferricyanide MFCs. These results show that internal resistance was not a predictor of overall maximum power densities, as the ferricyanide MFCs produced more power than the air–cathode MFCs, but also had higher internal resistances.

A comparison of the individual electrode resistances showed that the trends in total internal resistances were mostly a function of the cathode resistances, despite some variation in the anode resistances (Fig. 5b). The cathode resistances for the ferricyanide reactors increased in the same order as the internal resistances, with the brush having the lowest resistance (11 ± 1 mΩ m^2) among the three configurations and were also smaller than those calculated for the two

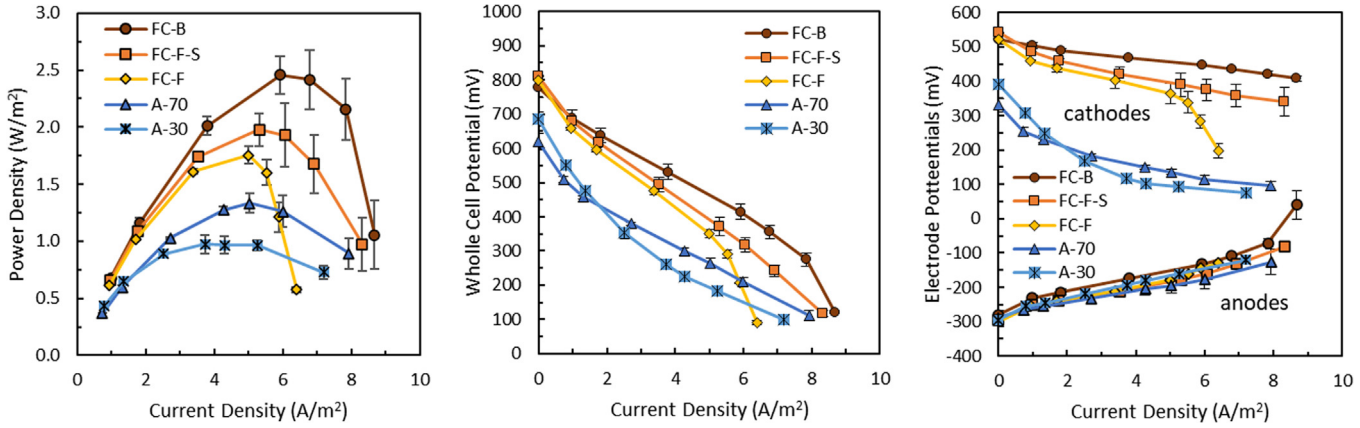

Fig. 3. (a) Power density, polarization curves – (b) whole-cell and (c) individual electrodes.

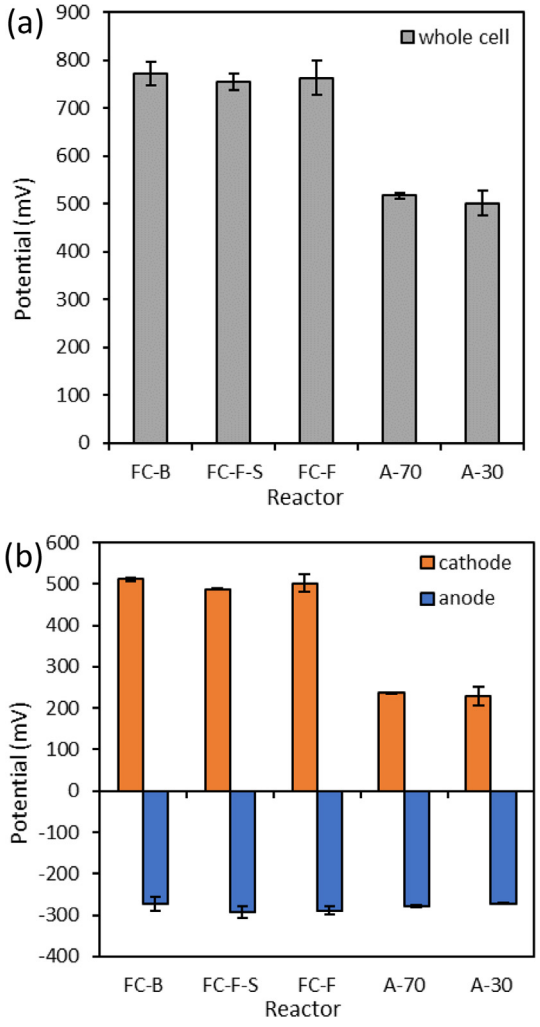

Fig. 4. (a) Working whole cell voltages, and (b) individual anode and cathode potentials obtained from the y-intercepts of the linearized polarization data using the EPS methods.

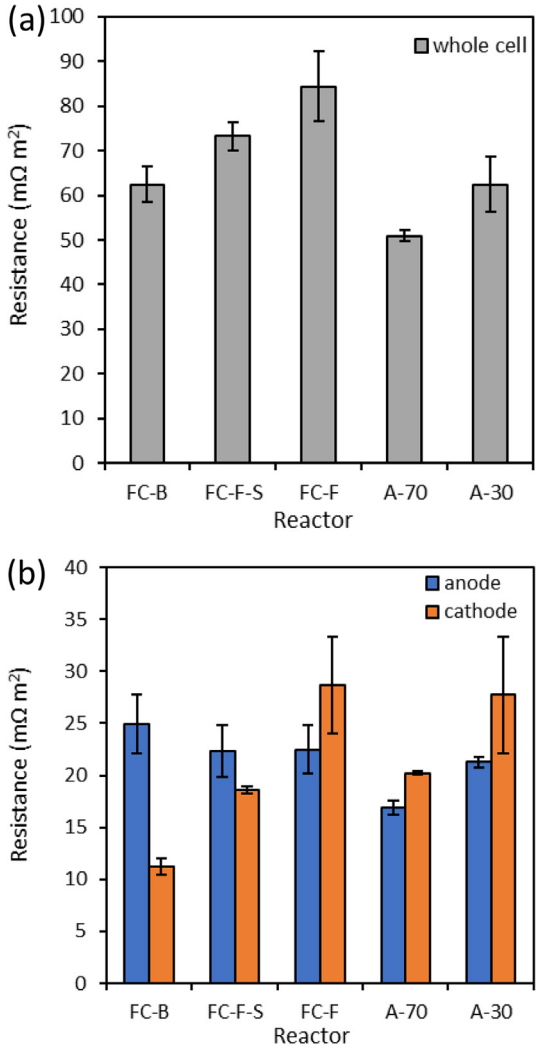

Fig. 5. (a) Whole cell internal resistances, and (b) anode and cathode resistances obtained from the slopes of the linear portions of the polarization data using the EPS method.

air–cathode types (20 ± 0 mΩ m^2, A-70; 28 ± 6 mΩ m^2, A-30). The anode resistances were not statistically different between the reactor configurations, either by cathode type (air vs ferricyanide), or specific cathode group (Tables A5–A8, Supporting Information) despite the lower average value for the A-70 anode (17 ± 1 mΩ m^2). In general, the anode resistances using oxygen as electron acceptor were the same or smaller than the anode resistances in the ferricyanide MFCs, suggesting any oxygen diffusion into the anolyte did not impact the anode resistance.

A comparison of the summed resistances shows that the catholyte solution resistance was a main distinguishing feature of the ferricyanide reactors compared to the air–cathode MFCs (Fig. 6). The anolyte resistances were similar in all reactors, with very small membrane

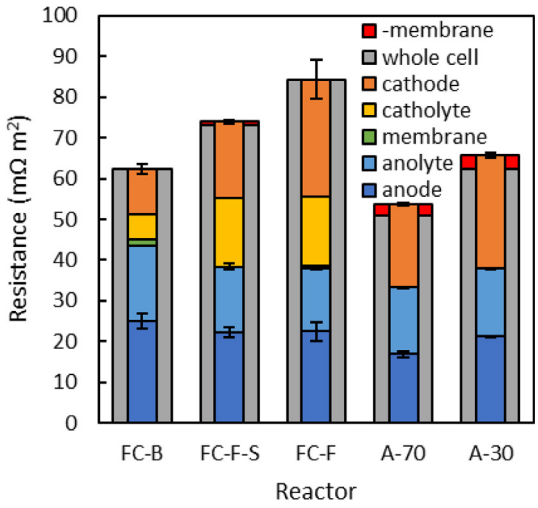

Fig. 6. Whole cell resistances compared to the sum of the anode, cathode, anolyte and catholyte (if present) resistances, compared to the total internal resistance. The membrane resistance is calculated as the difference between the whole cell and summed resistances.

resistances in the ferricyanide MFCs. The slightly negative values of two air–cathode MFCs is shown as a "membrane" resistance even though there was no membrane in the air–cathode MFCs, since this resistance term represents the difference in the summed electrode and solution resistances compared to the total internal resistance as shown in eq. (1).

3.4. Implications

While ferricyanide MFCs produce higher power densities than air–cathode MFCs (Fig. 3), their internal resistances were similar to or larger than those of the air–cathode MFCs (Fig. 6). The main reason for the higher internal resistance of the ferricyanide MFCs was the additional contribution of the catholyte to the internal resistance. The brush-cathode MFCs had a lower catholyte resistance due to the edge of the brush being placed closer to the membrane than that for the flat cathode. The position of the cathodes in ferricyanide MFCs are not always reported, and thus our analysis reveals these distances are important as they can substantially impact the overall internal resistance. The main reason for the higher power densities with ferricyanide here was the higher cathode potentials for the ferricyanide MFCs (500 ± 12 mV) compared to those for the air–cathode MFCs (233 ± 5 mV). This additional ~270 mV increased power despite the comparable anode potentials and other resistances.

The total internal resistance, as well as the anode and resistances measured here for the A-70 air cathode, were slightly larger than those reported by Rossi et al. (2019) (Table 2). In addition, the whole cell potentials were somewhat larger as well, resulting in a lower power density of 1.33 ± 0.14 W/m^2 here, as compared to the previously reported power density of 1.71 W/m^2. However, the power density for these air–cathode MFCs compares well to the average of 1.36 ± 0.20 W m^2 (n = 24) reported for a comparison of many different studies using the same cube-type brush-anode and air–cathode MFCs (Yang et al., 2017b). Despite differences in the performance of the cathodes, the sum of the anode and cathode resistances were similar for the three MFCs summarized in Table 2. While the internal resistance of the ferricyanide MFCs were slightly larger than those of both air–-cathode MFCs, the EPS analysis conclusively showed that the main difference for the much higher power production of the ferricyanide MFCs than the air–cathode MFCs was the much larger potentials produced by the ferricyanide catholyte compared to the air cathode. The higher power was possible as power is combination of the cell voltage and resistance (i.e. $P = U^2/R$) where R is the sum of the internal and external resistances. Thus, a higher U based on using ferricyanide was more critical to power production than the slightly higher internal resistance.

4. Conclusions

Comparison of different types of MFCs requires a careful analysis of internal resistances and the components of the internal resistance, as well as the working electrode potentials. Although ferricyanide MFCs produced higher power densities than those with air cathodes, their internal resistances were similar to or higher than those of the air–-cathode MFCs. The anode and cathode resistances were similar, with the main difference being the additional catholyte resistance in the ferricyanide MFCs. Therefore, for air–cathode MFCs to produce more power, the half-cell potentials for the cathode need to be increased to be closer to the thermodynamic limits.

CRediT authorship contribution statement

B.E.L. and K.L. conceived the idea, K.L. collected and provided data curation, B.E.L. provided project administration, and K.L., R.R., J.M.R. and B.E.L. analyzed and interpreted the data, discussed the results, and contributed to writing, reviewing, and editing the final manuscript.

Declaration of Competing Interest

The authors declare that they have no known competing financial interests or personal relationships that could have appeared to influence the work reported in this paper.

Acknowledgments

This research was funded by the Stan and Flora Kappe endowment, and Penn State University.

Table 2
Comparison of the best performing ferricyanide and air–cathode MFC characteristics compared to the performance of an air–cathode MFC examined by Rossi et al. (2019).

Characteristic	Component	Ferricyanide (FC-B) (This study)	Air cathode (A-70) (This study)	Air cathode (A-70) (Rossi et al., 2019)
Resistances	Internal	62 ± 4	51 ± 1	41 ± 1
	Anode	25 ± 3	17 ± 1	11 ± 1
	Cathode	11 ± 1	20 ± 0	15 ± 1
	Solution*	20 ± 0	17 ± 0	14
Potentials	Whole cell (mV)	773 ± 25	517 ± 6	531 ± 5
	Anode (mV)	–273 ± 18	–278 ± 3	–260 ± 3
	Cathode (mV)	511 ± 5	237 ± 1	271 ± 6
Performance	Maximum power (W/m^2)	2.46 ± 0.26	1.33 ± 0.14	1.71 ± 0.08
	Current at max power (A/m^2)	5.9 ± 0.3	5.0 ± 0.3	7.0 ± 0.2

*Sum of the anolyte and catholyte resistances.

Appendix A. Supplementary data

Supplementary data to this article can be found online at https://doi.org/10.1016/j.biortech.2020.123919.

References

Bretschger, O., Obraztsova, A., Sturm, C.A., Chang, I.S., Gorby, Y.A., Reed, S.B., Culley, D.E., Reardon, C.L., Barua, S., Romine, M.F., Zhou, J., Beliaev, A.S., Bouhenni, R., Saffarini, D., Mansfeld, F., Kim, B.-H., Fredrickson, J.K., Nealson, K.H., 2007. Current production and metal oxide reduction by *Shewanella oneidensis* MR-1 wild type and mutants. Appl. Environ. Microbiol. 73, 7003–7012.

Cario, B.P., Rossi, R., Kim, K.-Y., Logan, B.E., 2019. Applying the electrode potential slope method as a tool to quantitatively evaluate the performance of individual microbial electrolysis cell components. Bioresour. Technol. 287, 121418.

Cusick, R.D., Hatzell, M., Zhang, F., Logan, B.E., 2013. Minimal RED cell pairs markedly improve electrode kinetics and power production in microbial reverse electrodialysis cells. Environ. Sci. Technol. 47, 14518–14524.

Cusick, R.D., Kim, Y., Logan, B.E., 2012. Energy capture from thermolytic solutions in microbial reverse-electrodialysis cells. Science 335, 1474–1477.

Feng, Y., Yang, Q., Wang, X., Logan, B.E., 2010. Treatment of graphite fiber brush anodes for improving power generation in air-cathode microbial fuel cells. J. Power Sources 195, 1841–1844.

Hays, S., Zhang, F., Logan, B.E., 2011. Performance of two different types of anodes in membrane electrode assembly microbial fuel cells for power generation from domestic wastewater. J. Power Sources 196, 8293–8300.

He, H., Yuan, S.-J., Tong, Z.-H., Huang, Y.-X., Lin, Z.-Q., Yu, H.-Q., 2014. Characterization of a new electrochemically active bacterium, Lysinibacillus sphaericus D-8, isolated with a WO3 nanocluster probe. Process Biochem. 49, 290–294.

Hong, Y., Call, D.F., Werner, C.M., Logan, B.E., 2011. Adaptation to high current using low external resistances eliminates power overshoot in microbial fuel cells. Biosens. Bioelectron. 28, 71–76.

Katuri, K.P., Scott, K., Head, I.M., Picioreanu, C., Curtis, T.P., 2011. Microbial fuel cells meet with external resistance. Bioresour. Technol. 102, 2758–2766.

Koók, L., Nemestóthy, N., Bélafi-Bakó, K., Bakonyi, P., 2020. Investigating the specific role of external load on the performance versus stability trade-off in microbial fuel cells. Bioresour. Technol. 309, 123313.

Liu, H., Logan, B.E., 2004. Electricity generation using an air-cathode single chamber microbial fuel cell in the presence and absence of a proton exchange membrane. Environ. Sci. Technol. 38, 4040–4046.

Liu, Z.D., Du, Z.W., Lian, J., Zhu, X.Y., Li, S.H., Li, H.R., 2007. Improving energy accumulation of microbial fuel cells by metabolism regulation using *Rhodoferax ferrireducens* as biocatalyst. Lett. Appl. Microbiol. 44, 393–398.

Logan, B.E., Aelterman, P., Hamelers, B., Rozendal, R., Schröder, U., Keller, J., Freguiac, S., Verstraete, W., Rabaey, K., 2006. Microbial fuel cells: methodology and technology. Environ. Sci. Technol. 40, 5181–5192.

Logan, B.E., Rabaey, K., 2012. Conversion of wastes into bioelectricity and chemicals using microbial electrochemical technologies. Science 337, 686–690.

Logan, B.E., Rossi, R., Ragab, A.a., Saikaly, P.E., 2019. Electroactive microorganisms in bioelectrochemical systems. Nat. Rev. Microbiol. 17, 307–319.

Logan, B.E., Wallack, M.J., Kim, K.-Y., He, W., Feng, Y., Saikaly, P.E., 2015. Assessment of microbial fuel cell configurations and power densities. Environ. Sci. Technol. Lett. 2, 206–214.

Logan, B.E., Zikmund, E., Yang, W., Rossi, R., Kim, K.-Y., Saikaly, P.E., Zhang, F., 2018. Impact of ohmic resistance on measured electrode potentials and maximum power production in microbial fuel cells. Environ. Sci. Technol. 52, 8977–8985.

Lovley, D.R., 2012. Electromicrobiology. Ann. Rev. Microbiol. 66, 391–409.

O'Reilly, J.E., 1973. Oxidation-reduction potential of the ferro-ferricyanide system in buffer solutions. Biochim. Biophys. Acta 292, 509–515.

Pant, D., Bogaert, G.V., Smet, M.D., Diels, L., Vanbroekhoven, K., 2010. Use of novel permeable membrane and air cathodes in acetate microbial fuel cells. Electrochim. Acta 55, 7710–7716.

Pasternak, G., Greenman, J., Ieropoulos, I., 2018. Dynamic evolution of anodic biofilm when maturing under different external resistive loads in microbial fuel cells. Electrochemical perspective. J. Power Sources 400, 392–401.

Popat, S.C., Ki, D., Rittmann, B.E., Torres, C.I., 2012. Importance of OH^- transport from cathodes in microbial fuel cells. ChemSusChem 5, 1071–1079.

Ringeisen, B.R., Ray, R., Little, B., 2007. A miniature microbial fuel cell operating with an aerobic anode chamber. J. Power Sources 165, 5981–6597.

Rismani-Yazdi, H., Christy, A.D., Carver, S.M., Yu, Z., Dehority, B.A., Tuovinen, O.H., 2011. Effect of external resistance on bacterial diversity and metabolism in cellulose-fed microbial fuel cells. Bioresour. Technol. 102, 278–283.

Rossi, R., Cario, B.P., Santoro, C., Yang, W., Saikaly, P.E., Logan, B.E., 2019. Evaluation of electrode and solution area-based resistances enables quantitative comparisons of factors impacting microbial fuel cell performance. Environ. Sci. Technol. 53, 3977–3986.

Rossi, R., Hall, D.M., Wang, X., Regan, J.M., Logan, B.E., 2020. Quantifying the factors limiting performance and rates in microbial fuel cells using the electrode potential slope analysis combined with electrical impedance spectroscopy. Electrochim. Acta 348, 136330.

Rossi, R., Logan, B.E., 2020. Unraveling the contributions of internal resistance components in two-chamber microbial fuel cells using the electrode potential slope analysis. Electrochim. Acta 348, 136291.

Sander, M., Hofstetter, T.B., Gorski, C.A., 2015. Electrochemical analyses of redox-active iron minerals: a review of nonmediated and mediated approaches. Environ. Sci. Technol. 49, 5862–5878.

Santoro, C., Arbizzani, C., Erable, B., Ieropoulos, I., 2017. Microbial fuel cells: from fundamentals to applications. A review. J. Power Sources 356, 225–244.

Santoro, C., Kodali, M., Shamoon, N., Serov, A., Soavi, F., Merino-Jimenez, I., Gajda, I., Greenman, J., Ieropoulos, I., Atanassov, P., 2019. Increased power generation in supercapacitive microbial fuel cell stack using FeNC cathode catalyst. J. Power Sources 412, 416–424.

Wang, Z., Deng, H., Chen, L., Xiao, Y., Zhao, F., 2013. In situ measurements of dissolved oxygen, pH and redox potential of biocathode microenvironments using microelectrodes. Bioresour. Technol. 132, 387–390.

Watson, V.J., Logan, B.E., 2011. Analysis of polarization methods for elimination of power overshoot in microbial fuel cells. Electrochem. Commun. 13, 54–56.

Watson, V.J., Nieto Delgado, C., Logan, B.E., 2013a. Improvement of activated carbons as oxygen reduction catalysts in neutral solutions by ammonia gas treatment and their performance in microbial fuel cells. J. Power Sources 242, 756–761.

Watson, V.J., Nieto Delgado, C., Logan, B.E., 2013b. Influence of chemical and physical properties of activated carbon powders on oxygen reduction and microbial fuel cell performance. Environ. Sci. Technol. 47, 6704–6710.

Wei, J., Liang, P., Cao, X., Huang, X., 2010. A new insight into potential regulation on growth and power generation of *Geobacter sulfurreducens* in microbial fuel cells based on energy viewpoint. Environ. Sci. Technol. 44, 3187–3191.

Yang, L., Deng, W., Zhang, Y., Tan, Y., Ma, M., Xie, Q., 2017a. Boosting current generation in microbial fuel cells by an order of magnitude by coating an ionic liquid polymer on carbon anodes. Biosens. Bioelectron. 91, 644–649.

Yang, W., Kim, K.-Y., Saikaly, P.E., Logan, B.E., 2017b. The impact of new cathode materials relative to baseline performance of microbial fuel cells all with the same architecture and solution chemistry. Energy Environ. Sci. 10, 1025–1033.

Yang, W., Logan, B.E., 2016. Immobilization of a metal–nitrogen–carbon catalyst on activated carbon with enhanced cathode performance in microbial fuel cells. ChemSusChem 9, 2226–2232.

Yi, H., Nevin, K.P., Kim, B.-C., Franks, A.E., Klimes, A., Tender, L.M., Lovley, D.R., 2009. Selection of a variant of *Geobacter sulfurreducens* with enhanced capacity for current production in microbial fuel cells. Biosens. Bioelectron. 24, 3498–3503.

Yilmazel, Y.D., Zhu, X., Kim, K.-Y., Holmes, D.E., Logan, B.E., 2016. Electrical current generation in microbial electrolysis cells by hyperthermophilic archaea *Ferroglobus placidus* and *Geoglobus ahangari*. Bioelectrochemistry 119, 142–149.

Zhang, L., Zhou, S., Zhuang, L., Li, W., Zhang, J., Lub, N., Deng, L., 2008. Microbial fuel cell based on *Klebsiella pneumoniae* biofilm. Electrochem. Commun. 10, 1641–1643.

Zou, L., Qiao, Y., Wu, X.-S., Ma, C.-X., Li, X., Li, C.M., 2015. Synergistic effect of titanium dioxide nanocrystal/reduced graphene oxide hybrid on enhancement of microbial electrocatalysis. J. Power Sources 276, 208–214.

Zuo, Y., Xing, D., Regan, J.M., Logan, B.E., 2008. Isolation of the exoelectrogenic bacterium *Ochrobactrum anthropi* YZ-1 by using a U-tube microbial fuel cell. Appl. Environ. Microbiol. 74, 3130–3137.